

Frédéric Fabry  
McGill University, Montreal, Quebec, Canada

## 1. REFRACTIVITY AND IHOP\_2002

Refractivity measurements by radar (Fabry et al. 1997; Fabry 2004) offer us our first glimpse at the 2-D structure of near-surface moisture at the mesoscale. While most moisture measurements until now had been limited to point values and vertical profiles, refractivity measurements allow us to observe the time evolution of moisture field in the same way that radar reflectivity made possible the study of the mesoscale structure of precipitation.

During IHOP\_2002, seven weeks of refractivity data were collected using the NCAR S-Pol radar. These confirmed the ability of refractivity to map the air masses and some of their characteristics (Weckwerth et al. 2005) as well as the potential of refractivity data for research and operational use. In parallel, very few researchers have been exposed to refractivity imagery and know what kind of information one can obtain from it. This paper illustrates some of the measurements made in Oklahoma in an attempt to both demonstrate their value and give potential users a better feel for what to expect. First, a general overview of the types of measurements possible is presented. My attention will then focus on a case study of convection initiation at the intersection between the dry line and a cold front as an excuse to study moisture variability and storm initiation.

## 2. TYPES OF MEASUREMENTS

Refractivity is measured by monitoring the travel time of radar waves between the radar and fixed targets on the ground. Changes in the phase of a fixed target can be linked to slight changes to the speed of light, from which the refractive index  $n$  and the refractivity  $N$  of air can be inferred. In the troposphere,  $N$  is a function of the pressure  $P$  (hPa), the temperature  $T$  (K), and the vapor pressure  $e$  (hPa) following

$$N = 10^6 (n - 1) = 77.6 \frac{P}{T} + 373000 \frac{e}{T^2} = N_{dry} + N_{wet} .$$

Two types of images were made. The first is the actual field of  $N$ . Although the density term  $N_{dry}$  is larger than the moisture term  $N_{wet}$ , most of the spatial variability observed in  $N$  fields is caused by  $N_{wet}$ . Therefore, given representative values for  $P$  and  $T$ , one can use  $N$  to derive  $e$  and hence the dew point temperature  $T_d$ . In the  $N$  images to follow, the color scale has two sets of units:

one is for refractivity, which is the quantity that is really being measured, and one is for  $T_d$  which is being derived using surface temperature and pressure data from the nine surface stations within 60 km of S-Pol.

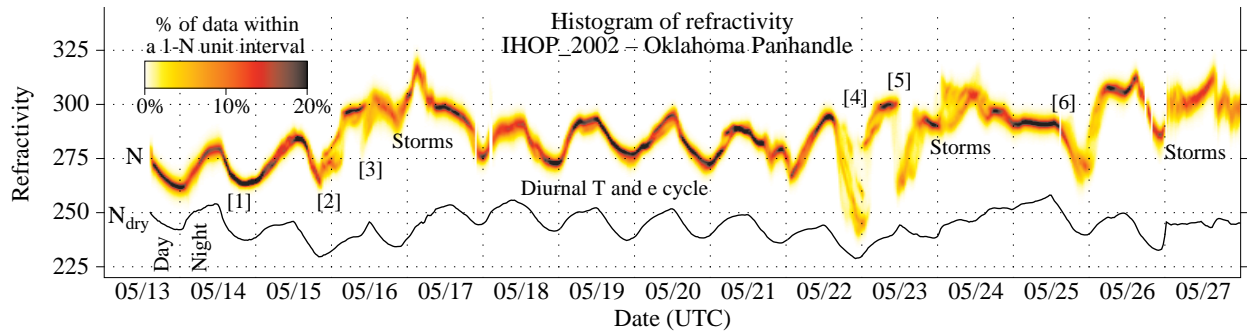
The second type of image is the scan-to-scan  $N$  change map. This map is counter-intuitively more accurate than the  $N$  map and is especially useful to single out regions where  $dN/dt$  is changing such as faint boundaries.

At the S-Pol site, ground targets were typically observed up to 30 km range, except towards the NW quadrant where, after a short gap caused by the Beaver River valley, they were seen up to 60 km range. Because  $N$  and  $dN/dt$  maps are made using ground targets, the data coverage is much smaller than for reflectivity or Doppler velocity. Nevertheless, it is large enough to allow a variety of observations to be made over the seven week period of IHOP\_2002.

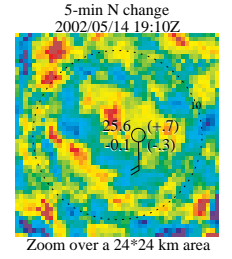
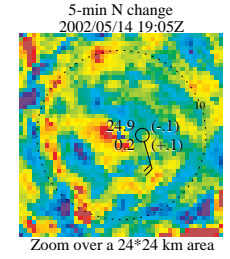
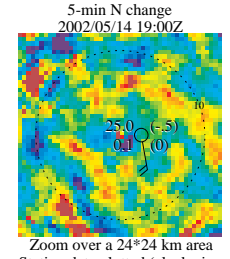
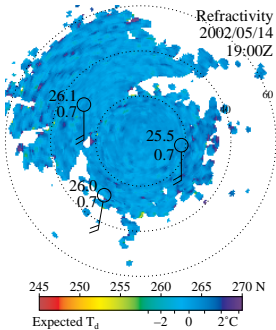
## 3. HIGHLIGHTS OF THE FIELD PROJECT

The top of Figure 1 shows the histogram of refractivity observed as a function of time. It illustrates the diurnal cycle of  $N$  data and the range of values being observed at any time, with darker narrow areas corresponding to very uniform conditions and wide or multimodal lighter areas being indicative of noticeable gradients in moisture within the small data coverage area. Since it covers the whole field experiment, it gives an unbiased view of the refractivity variability over a long period and allows the reader to get a better appreciation of the frequency of occurrence of the examples to follow.

Twelve sets of examples of refractivity imagery are then provided in the bottom part of Figure 1 associated with different signatures in the histogram. Examples cover a wide variety of phenomena: larger scale moisture boundaries such as those associated with fronts (note [5]), drylines and other convergence lines ([4], [12] and [13]), gust fronts and outflows ([8], [10], [11]), or less sharp gradients of unclear origin ([7] and [10]); boundary layer (BL) phenomena such as rolls ([14]), more cellular structures ([1]), and uneven moistening of the BL by surface fluxes ([6]); and finally, nocturnal waves ([9] and [10]). As this list suggests, refractivity data could hence be of considerable interest not only to meteorologists concerned with convection initiation (CI), but also to researchers in boundary layer processes. Of particular interest for CI was the observation that, very often, convergence lines could be detected in refractivity prior to having been detected in reflectivity ([4], Weckwerth et al. 2004).



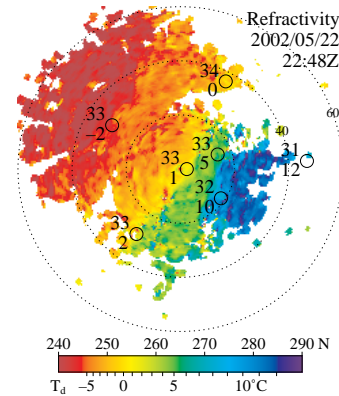
[1] Day-time data in a uniform air mass. Although no large-scale  $N$  gradients are visible (first image), small-scale boundary layer structures may be tracked on the time series of 5-minute refractivity differences (far right), although considerable change occurs.



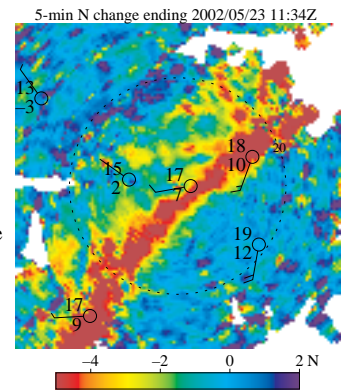
[2] Gradual sharpening of a moisture gradient associated with a refractivity fineline. Similar to but not as impressive as [4].

[3] Cold front passing over the area with a dew point decrease behind it.

[4] One of the banner days for refractivity, as a main dryline and a few secondary drylines gradually built up over the area. Interestingly, the build-up of the boundaries was detected with refractivity before one could clearly observe any refractivity finelines. This might be related to the fact that it takes time for the updrafts associated with the convergence lines to lift enough insects to permit their detection using refractivity.



[5] Image of the change in refractivity over a 5-min period during the passage of a cold front over a 60 by 60 km area. This image reveals that, behind the initial change in temperature and moisture along the front boundary is a 15-km wide transition zone over which the refractivity (associated with the dew point and real temperatures) continues to decrease until it reaches its final value.



[6] Thanks to very weak winds and uneven rain in the previous days (first image), we observed the gradual appearance of regions with different humidity (far right) solely caused by the variable surface moisture fluxes as a function of soil moisture.

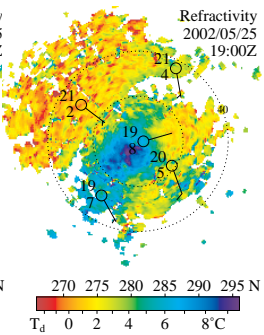
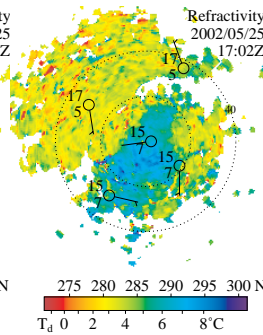
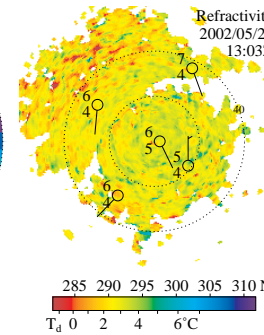
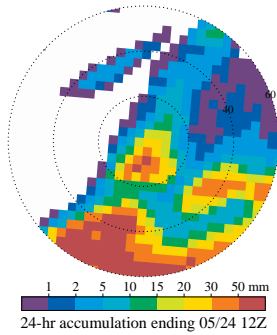
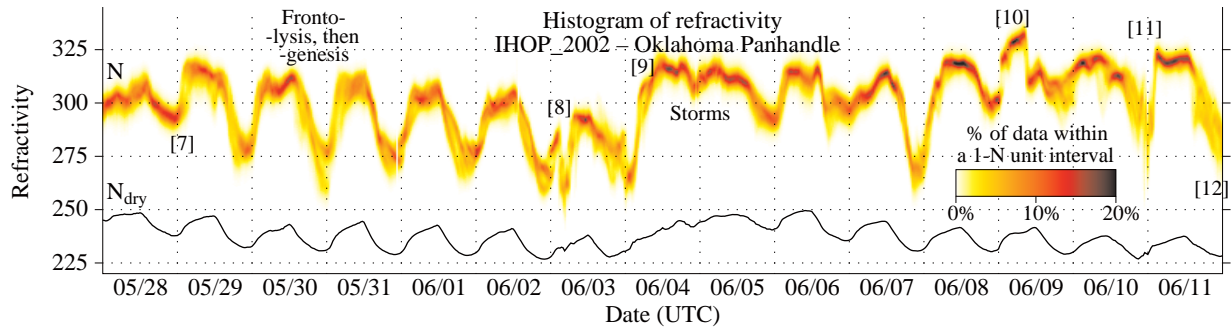
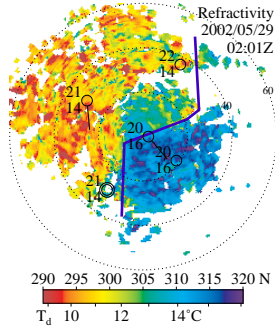


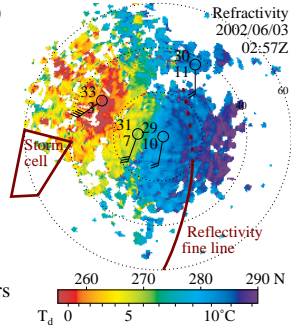
FIG. 1. Top: Histogram of refractivity as a function of time observed by the S-Pol radar in the Oklahoma Panhandle from the 13 May to 25 June 2002. The difference between the  $N_{dry}$  curve and the values associated with shades of yellow and red is proportional to the amount of moisture measured near the surface. Bottom: Mini case studies of individual events annotated on the histogram plot. These include a short text description and a variety of radar data (surface refractivity, 5-min surface refractivity change, and PPIs of reflectivity and of Doppler velocity) and surface observations (often plotted on the refractivity maps, sometimes plotted on the side in the form of a time series). The first page presents the first 14 days of IHOP\_2002; two more pages do the rest.



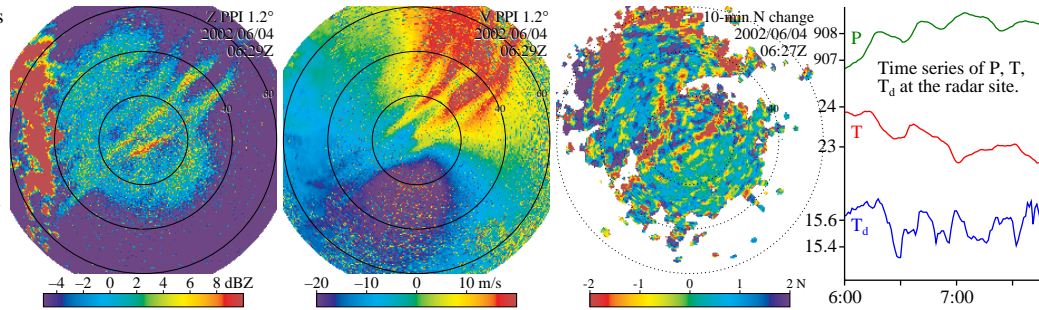
[7] Sudden pulse of surface moisture occurring at the beginning of the night. In this area, nighttime moistening is often associated with the passage of an air-mass boundary coming from the SE early in the night. By contrast, the daytime drying occurs mainly by vertical mixing. Also note the large difference between N-derived dew point temperatures – representative of data at about 20 m – and the actual surface measurements.



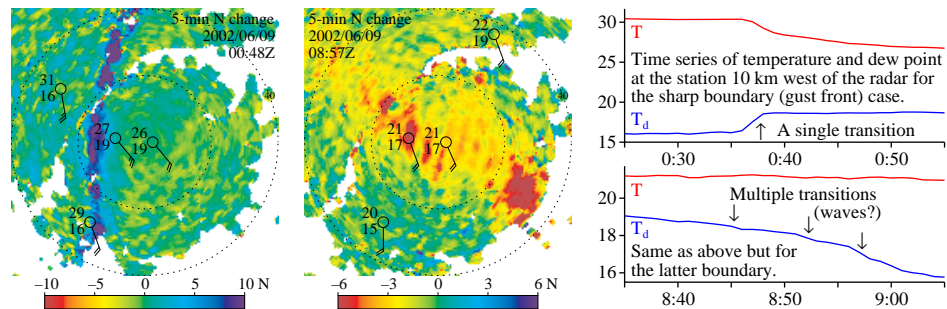
[8] (Multiple?) storm outflow(s) from a line of thunderstorms SW of the radar site. While the reflectivity map shows only one fineline associated with the outflow (solid and dotted line), the refractivity map (right) suggests the presence of multiple boundaries with only an extremely faint refractivity contrast colocated with the reflectivity fineline. In this case, the outflow is relatively warm and dry; in others (e.g. [11]), it is cool and humid.



[9] Nighttime bore as seen on (left to right) reflectivity, Doppler velocity and 5-min refractivity change. At this time, the bore is barely detectable on refractivity as pressure waves show some correlation with dew points. Case analyzed by Koch et al. (2003).



[10] Two examples of refractivity boundaries: a sharp temperature and moisture boundary (caused here by a gust front), and a diffuse moisture transition a few hours later. Both the refractivity change maps and the surface data (far right) show the different nature of the boundaries. The latter example displays hints of a wave structure within it, not an uncommon occurrence for nighttime boundaries.



[11] Very high range of refractivity values caused by the presence of multiple storm outflows. Such conditions cause problems to the algorithm retrieving refractivity fields; hence, data quality is poorer than usual and the field shows considerable fragmentation.

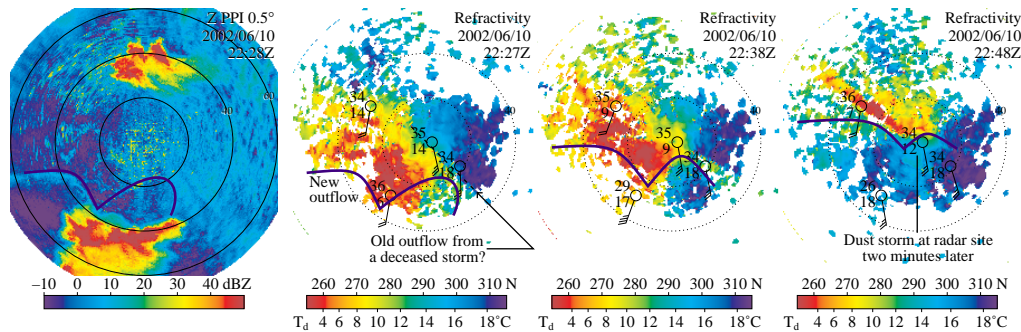
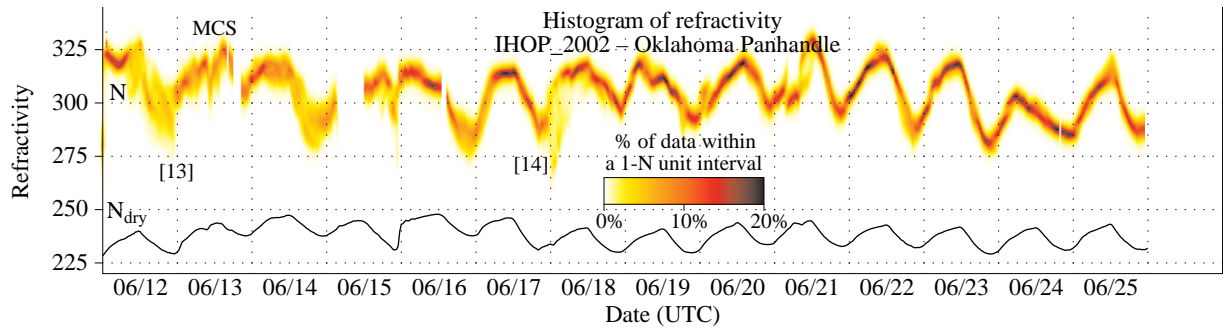
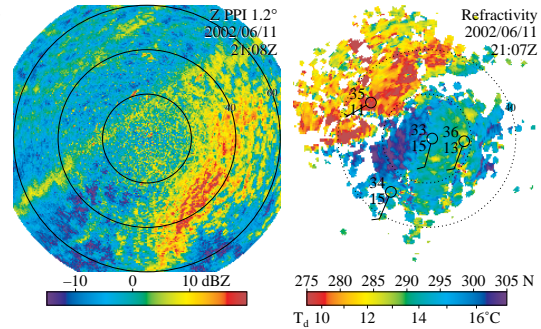
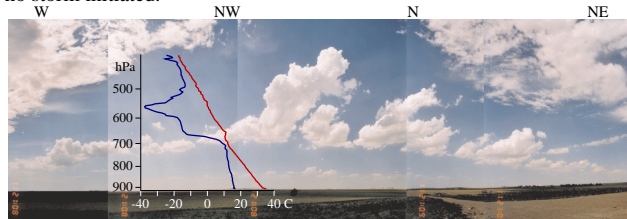


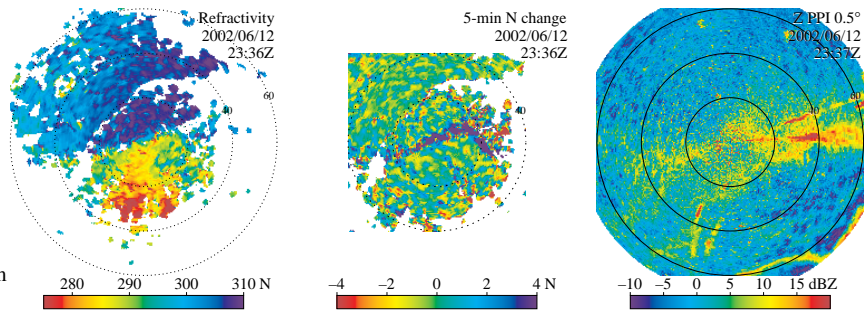
FIG. 1 (cont)



[12] Here, the relatively wide range of refractivity values observed is associated with the presence of a convergence line just NW of the radar site (visible on reflectivity as a fineline (right) as well as on refractivity (far right)). Although clouds poked through the capping inversion (see photo below from S-Pol), no storm initiated.



[13] On this day, a weak low pressure system was forming over S-Pol. A persistent slow-moving dry pocket drifted to the southern edge of the refractivity coverage. By 2336Z, a boundary had built up and was moving south (see the refractivity and refractivity change maps on the right). In parallel, a gust front coming from the south can be seen on the refractivity map (far right) 60 km from the radar. These two boundaries collided 45 min later and a severe thunderstorm initiated 30 km east of S-Pol as a result.



[14] Example of smaller scale variability in refractivity caused by the boundary layer structure on a sunny and windy day. At this time (about 14:00 solar time), BL rolls can be observed on reflectivity (first image). On refractivity (second image), when two images are averaged (19:59 and 20:04) to remove the cross-roll variability, one may observe some along-roll refractivity structure superposed on a stronger larger scale moisture variability. The 5-min refractivity change map (far right), that enhances cross-wind N variability, reveals the presence of cross-roll N structure as well.

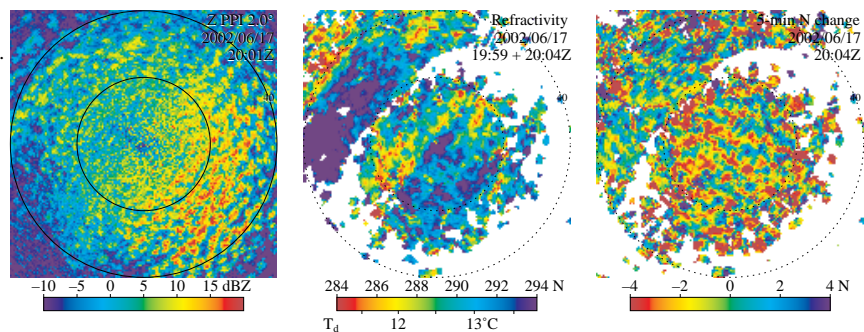


FIG. 1 (cont)

#### 4. CASE STUDY OF CONVECTION INITIATION

Cases of daytime CI within the short range of the refractivity measurements were relatively rare during IHOP\_2002. Most of them were clearly associated with the collision of two boundaries (e.g., [13]). Perhaps the most interesting event, if not the most spectacular, occurred on the evening of 11 May 2002.

In the hours preceding the official start of IHOP\_2002, the crew of the National Center of Atmospheric Research (NCAR) S-Pol radar monitors

the interaction between the dry line, boundary layer linear signatures that might be associated with unusually large convective rolls, and an approaching cold front. Suddenly, convection initiation (CI) occurs, at first as a line of thunderstorms along the cold front (20:30 UTC, or 14:30 LST). While more cells of various magnitude develop along the cold front (21:30 – 01:30), isolated cells are triggered a few tens of kilometers east of the dry line and south of the front (22:00 – 22:30), and then progressively closer to the triple point (01:00) where the cold front and the dry line meets (Fig. 2).

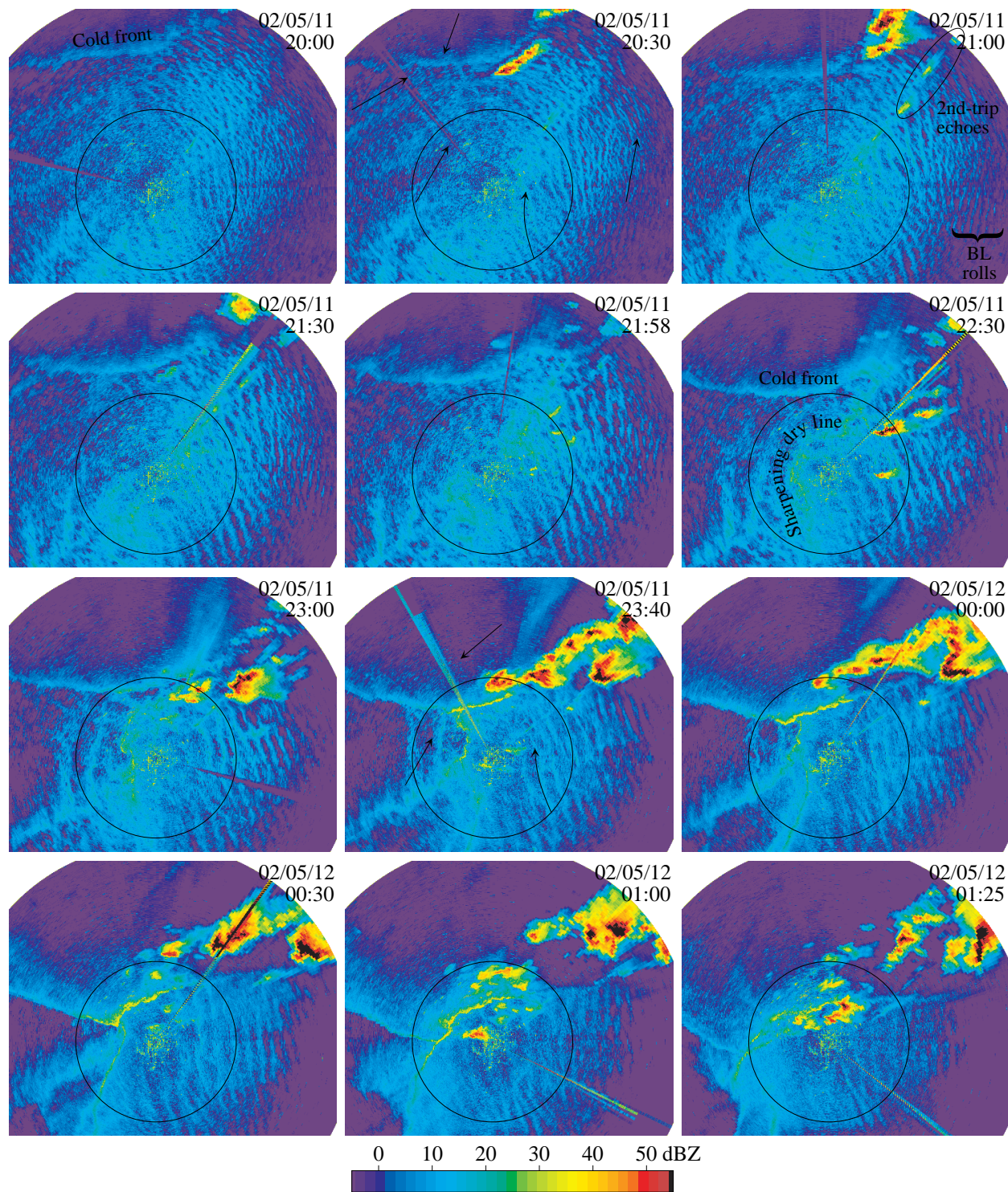


FIG. 2. Time sequence of  $0^\circ$  PPIs of reflectivity measured by S-Pol on 11 May 2002. In each individual image, the circle indicates a range of 60 km from the radar. On two images, arrows show the direction and relative strength of Doppler-measured winds.

The strongest convection on that day was clearly associated with the cold front. In the warm wet sector, the explanation for the small isolated cells is not as clear based on reflectivity data alone. Since IHOP\_2002 had

not yet started on 11 May, there are only a limited number of data sources beyond the radar itself to help understand the nature of this event. Fortunately, Doppler and refractivity data provide a partial answer.

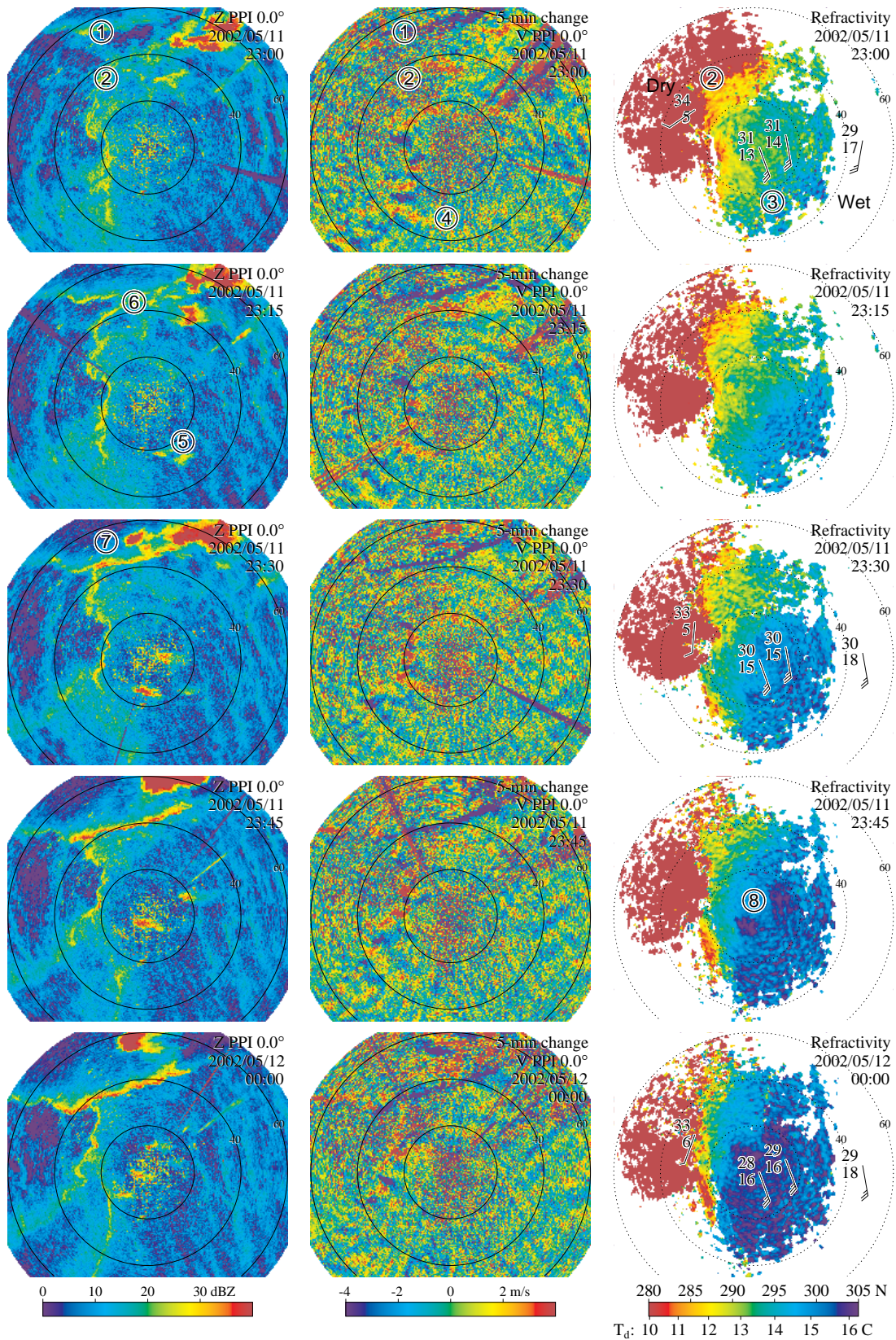


FIG. 3. Time sequence of radar PPIs ( $0^\circ$  elevation) of reflectivity (left), 5-min change in Doppler velocity (middle) to emphasize weak boundaries and other dynamical signatures that might otherwise pass unnoticed, and refractivity (right) from 23:00 to 00:00 UTC. Annotations (1 to 8) are discussed in the main text.

Figure 3 focuses on the time period between 23:00 and 00:00 UTC. By that time, the cold front (annotation (1) in Fig. 3) and the dry line (2) are well observed on the reflectivity, Doppler velocity and refractivity fields. The area east of the dry line and south of the front is undergoing a gradual moistening (3) that does not seem to be associated with any clear air mass transition. Thanks to a sizable wind shear across the dry line, we can observe the presence of waves on that dry line, some of which that appear to extend or be connected with other weaker waves in the wet sector (4). Two families of CI *modus operandi* occur during that time. First, cells (5) seem to occur more or less randomly as a result of the gradual moistening (3) and perhaps also of the waves (4) observed in the moist sector. Then, other cells are clearly forced by the strong convergence on the cold front, or occur as a result of the collision between two boundaries (6) (7). The resulting precipitation then humidifies the BL, creating moist patches (8) that are then advected and gradually mixed with neighboring parcels.

An observation of particular interest is that while there is some correlation between the increase in moisture at the 10-20 km scale and that of CI, it is very difficult to find local maxima at smaller scales that would explain why initiation occurred at one particular location and not another. There are two possible explanations to this ascertainment. On one end, it suggests that moisture variability at scales smaller than 10 km is not important for CI and that the exact location of CI is dictated by either dynamics or temperature fluctuations. On the other end, moisture variability at the surface at small scales may not mimic the variability near the top of the BL where the CI is triggered.

## 5. DYNAMICS, THERMODYNAMICS, AND CI

Because of the lack of data from other sensors, we will never know which of the two scenarios presented above is the correct one for 11 May 2002. However, one may try to evaluate which is the most probable by studying many other events and trying a statistical approach. In an attempt to determine which of the above-mentioned scenario is the most probable, in-situ measurements in the boundary layer made by the University of Wyoming King Air during IHOP\_2002 were analyzed to determine the variability in moisture, temperature, and vertical velocity as a function of scale. All flights made during the time period between 18 and 22 UTC (solar afternoon) were considered, and flight legs made either near the surface (60 to 150 m above ground level) or in the top half of the boundary layer were processed. For each of these legs, data were averaged over a 1-km distance and contrasted with nearby data up 20 km away.

The first question that was investigated was how different is the variability in temperature and especially moisture in the upper BL as opposed to in the lower BL. Data collected during flights where measurements at

both levels were acquired on the same flight were considered. They show that while temperature variability is marginally reduced in the upper BL compared to near the surface, moisture variability is enhanced significantly, especially at small scales. As a result, the analysis that follows will rely exclusively on aircraft data collected near the top of the BL.

If BL humidity or temperature change, so will the energy of convective inhibition (CIN). Given soundings in near-CI conditions, one can compute how the observed variability in humidity and temperature will map into variability in CIN, and therefore determine how important this variability is for the initiation of convection. The change in CIN with temperature and moisture is a function of the magnitude of the CIN energy itself as well as of the profile selected. Given the focus on CI, ten soundings made near S-Pol in conditions of expected CI were selected. Surface parcels were then warmed and/or warmed and moistened until CIN equals zero, simulating conditions where CI would occur. These modified profiles were used as starting points to our analysis. Then, surface humidity or temperature was lowered by the measured 1- $\sigma$  and 2- $\sigma$  variability in humidity and temperature at a particular scale determined from the analysis of the aircraft data, and new CIN values were computed for those parcels. It was then assumed that these computed CIN values represent the amount of CIN variability associated with the observed variability in temperature and moisture.

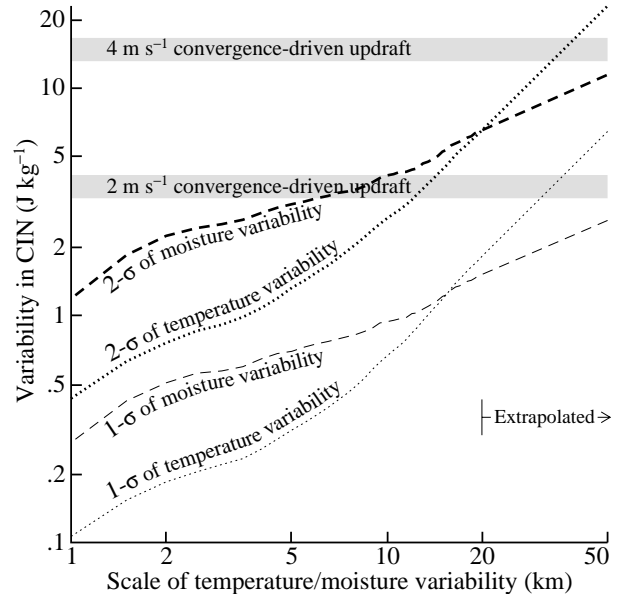


FIG. 4. Effect of the observed variability in temperature (dotted line) and moisture (dashed line) on convective inhibition (CIN) in the upper BL as a function of the scale over which that variability is observed. The contributions to CIN variability of the one- and two-standard deviations of the distribution of temperature and moisture observed at a given scale are contrasted with the effect of 2 and 4  $\text{m s}^{-1}$  convergence-driven updrafts using the formula of Crook and Klemp (2000).

The result of this exercise is shown in Fig. 4. One can observe that at scales smaller than 15 to 20 km, the variability in humidity has a greater effect on CIN than the variability in temperature. At larger scales, the increasing temperature variability has a greater impact on CIN. Including dynamics changes the picture considerably: a relatively modest convergence-driven updraft will have a much bigger impact on the exact location of CI than moisture or temperature variability. Therefore, at scales smaller than a few tens of kilometers, detailed knowledge of dynamics becomes a lot more important than that of temperature and of moisture. This result is not very surprising as it confirms the well-known observation that CI generally occurs near a convergence boundary. In a sense, this could be considered as good news, because with the existing atmospheric observation sensors, it is much easier to make small-scale measurements of dynamics than of thermodynamics. On the other end, the extreme sensitivity to dynamics means that only very precise measurements of convergence and updrafts will allow accurate CI prediction.

When all these three parameters are looked together, it appears that moisture variability only has a relatively small impact on CI. This explains why one had problems relating CI on the 11 May event with small-scale moisture pockets (Fig. 3). IHOP\_2002 sought to find out whether “improved characterization of the water vapor field will result in significant, detectable improvements in warm-season QPF skill”. As far as convection initiation is concerned, the answer to the question appears to be “in general, no”, at least in the Oklahoma Panhandle. In much wetter places where humidity variability will be considerably larger, such as in Florida, the answer might be different. Only in areas of limited dynamical forcing will moisture variability have a significant effect, such as in the example shown by annotation (5) in Fig. 3. Note that even in that case, help from dynamics appear to have been essential (annotation (4)). Of course, once initiation occurs, moisture will be a key factor in determining the strength of that convection.

One might conclude from this exercise that measurements of refractivity would then offer little information on CI because of the apparent limited impact of moisture variability on CI: the key to CI prediction is and remains the detection of convergence zones. Such a conclusion would neglect the fact that refractivity measurements are extremely valuable to detect these convergence regions: in many instances, convergence lines were observed on refractivity sometimes several hours before a reflectivity fine line could be identified. For example, Fig. 5 shows multiple refractivity boundaries early on 11 May that cannot be identified on the reflectivity data (Fig. 2). An ironic conclusion of this work is that although the interest on refractivity has been centered on its ability to estimate moisture, high resolution refractivity measurements may

end up being crucial for CI prediction solely to resolve the otherwise hidden small-scale dynamics!

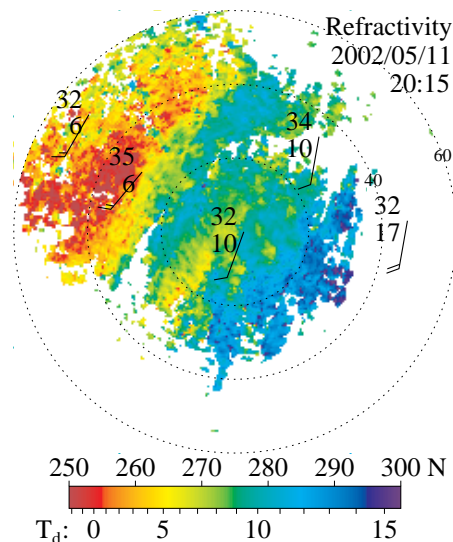


FIG. 5: Example of a refractivity field at a time when the dry line has not yet collapsed into a single line visible on radar reflectivity (see Fig. 2). The refractivity scale also shows the corresponding dew point temperatures given the average pressure and temperature conditions at 20:15 UTC.

## 6. ACKNOWLEDGEMENTS

I thank Joe Vanandel and Bob Rilling from NCAR for their help in adapting the refractivity code on S-Pol and rerunning the analysis post-facto, and Tammy Weckwerth, Crystalline Pettet, and Ned Chamberlain for the many surface stations near S-Pol used in this study. My sincere thanks to the hard work and diligent effort of the University of Wyoming and National Center for Atmospheric Research staff fielding and pre-processing the data from their instruments within and beyond the National Science Foundation deployment pool.

## 7. REFERENCES

- Crook, N.A., and J.B. Klemp, 2000: Lifting by convergence lines. *J. Atmos. Sci.*, **57**, 873-890.
- Fabry, F., et al. 1997: On the extraction of near-surface index of refraction using radar measurements of ground targets. *J. Atmos. Oceanic Technol.*, **14**, 978-987.
- Fabry, F., 2004: Meteorological value of ground target measurements by radar. *J. Atmos. Oceanic Technol.*, **21**, 560-573.
- Koch, S.E., et al. 2003: Multisensor study of a dual bore event observed during IHOP. Preprints, 10<sup>th</sup> Conf. Mesoscale Processes, Portland OR, paper 14.3.
- Weckwerth, T.M., et al., 2004: An overview of the International H<sub>2</sub>O Project (IHOP\_2002) and some preliminary highlights. *Bull. Amer. Meteorol. Soc.*, **85**, 253-277.
- Weckwerth, T.M., C.R. Pettet, F. Fabry, S. Park, J.W. Wilson, and M.A. LeMone, 2005: Radar refractivity retrieval: Validation and application to short-term forecasting. *J. Applied Meteor.*, in press.